Journal of Engineering Mechanics and Machinery (2024)
Clausius Scientific Press, Canada

DOI: 10.23977/jemm.2024.090218
ISSN 2371-9133 Vol. 9 Num. 2

Investigation of the conjugate heat transfer and cooling mechanism of film cooling holes with different ellipticities

Dongxu Zhang[1,a], Kaitai Feng[1,b,*], Haobo Yu[1,c], Zhenyu Xin[1,d], Xubo Yang[1,e], Zhixun Wen[2,f]

[1]College of Mechanical and Electrical Engineering, Shaanxi University of Science & Technology, Xi'an, Shaanxi, 710021, China
[2]School of Mechanics, Civil Engineering and Architecture, Northwestern Polytechnical University, Xi'an, 710072, China
[a]zhangdongxu@sust.edu.cn, [b]220511017@sust.edu.cn, [c]2205121217@sust.edu.cn, [d]xinzhenyu@sust.edu.cn, [e]220512078@sust.edu.cn, [f]zxwen@nwpu.edu.cn
[*]Corresponding author

Keywords: Film cooling, film cooling hole, ellipticity, conjugate heat transfer

Abstract: The cooling characteristics and cooling mechanisms of various elliptical film cooling holes were analyzed at blowing ratios of 0.5, 1.0, and 1.5. Five different elliptic film cooling hole structures were obtained based on the cylindrical hole model by varying the aspect ratio of the film cooling holes. To examine the cooling performance of individual film cooling apertures under both adiabatic and conjugate heat transfer conditions, numerical simulations were carried out using computational fluid dynamics (CFD) and conjugate heat transfer (CHT) techniques. The cooling mechanisms were elucidated based on these simulations. The results indicate that elliptical film cooling apertures exhibit the maximum cooling efficiency at a moderate blowing ratio. A decrease in ellipticity leads to a structural alteration in the shear layer vortex within the flow field. Apertures with lower ellipticity induce more robust shear layer vortices, improving the cooling effectiveness. Additionally, among the analyzed elliptical holes, those with an ellipticity of 0.5 exhibited superior comprehensive cooling effectiveness and film coverage efficiency, showing the best film cooling performance.

1. Introduction

Turbine blades are vital high-temperature components that enhance the thermal efficiency of gas turbines, ensuring continuous and reliable operation under extreme conditions. To improve the thermal and physical properties of blade materials and thermal barrier coatings [1,2], film cooling technology has been widely adopted due to its simplicity and effectiveness [3-5]. Increasing the inlet air temperature is widely acknowledged as one of the most efficient approaches for enhancing gas turbine performance [6,7]. The inlet air temperature of modern gas turbines has surpassed 2000 K [8], greatly exceeding the temperature tolerance of blade materials. Film cooling helps to prevent direct contact between the blade surface and the hot gas, thereby assisting in blade cooling.

Extensive research has concentrated on the geometric structure and heat transfer performance of film cooling holes to improve the cooling efficiency of this technology and optimize the use of cooling

media. The aim is to enhance the cooling effectiveness by optimizing the flow structure within the holes and minimizing the interaction between the cooling jet and the high-temperature mainstream [9-17]. Fu et al.[15] performed a comparative study on the aerodynamic and heat transfer characteristics of standard cylindrical holes versus fan-shaped holes at specified blowing ratios. Fan-shaped holes demonstrated superior overall cooling ability at high air-to-volume ratios, characterized by kidney-shaped vortices in the flow field. Research by Kusterer et al. [18] indicates that 77% of the overall cooling efficiency of the NEKOMIMI film cooling hole is due to the optimized flow arrangement in the secondary flow of the film cooling, while 23% results from heat conduction in the NEKOMIMI configuration material. Wang et al. [19] introduced a Rupert-shaped film cooling hole and compared its film cooling effectiveness with that of cylindrical holes. Overall, the design of noncylindrical holes effectively prevented severe film detachment at high blowing ratios and exhibited lower jet exit kinetic energy, weaker vortex intensity, better film coverage, and thus superior cooling performance compared to cylindrical holes.

However, conventional adiabatic investigations have constraints, as adiabatic cooling efficiency alone fails to fully grasp the holistic cooling efficacy of film cooling. The combined influences of convective heat transfer within the apertures, solid heat conduction, and external film cooling impact the internal temperature gradient of the blades. [15,20-26]. The interaction between convective heat transfer within the orifices and external film cooling modifications to the geometric structure of the film cooling holes significantly impacts the overall flow field structure and heat transfer performance [23,27-29]. Therefore, conjugate heat transfer analysis (CHT) has become the primary research method for examining the overall cooling performance of films. Mahmood Silieti et al. [26] conducted a comparative study between adiabatic and conjugate heat transfer CFD models of film cooling. The research findings highlight substantial differences in temperature predictions between the conjugate and adiabatic heat transfer models, emphasizing the need to consider metal heat conduction when predicting wall temperatures. Zhou et al. [20] introduced a coupled heat transfer decoupling approach to unravel the intricate interactions between external and internal cooling within composite cooling structures. Using the decoupled model, a quantitative assessment was conducted on the contributions of internal and external cooling to the overall cooling efficiency.

Nonetheless, concerning noncylindrical holes with minor geometric variations, there remains a research gap regarding the optimization of hole geometry parameters and a comprehensive study of the most suitable operating conditions. Thus, we analyzed the operating mechanisms of flow field structures under different conditions is crucial for understanding the relationship between the optimal overall cooling performance and the structural parameters of film cooling holes. By using CFD and CHT simulations to study the effects of film cooling and convective heat transfer on the temperature gradient of the sample, thermal physical boundaries are provided for the study of the mechanical properties of film pores in real aerodynamic environments, achieving joint optimization between film pore structure parameters and optimal performance.

2. Numerical simulation methodology

2.1. Geometric model and boundary conditions

This study performed both adiabatic and conjugate heat transfer analyses for various elliptical film cooling holes to evaluate the complete cooling capability of elliptical film cooling orifices. The analysis model employed a single-hole flat plate model for the computations. The computational domain was segmented into fluid and solid regions, with the fluid region further subdivided into a high-temperature mainstream region and a low-temperature coolant region. The material for the solid region was specified as a DD6 nickel-based superalloy, with a melting point range of 1615.15 K to 1672.15 K and a density of 8780 kg/m ^{3}. The heat transfer efficiency and heat capacity per unit mass

of this alloy at high temperatures were obtained from relevant material handbooks[30].

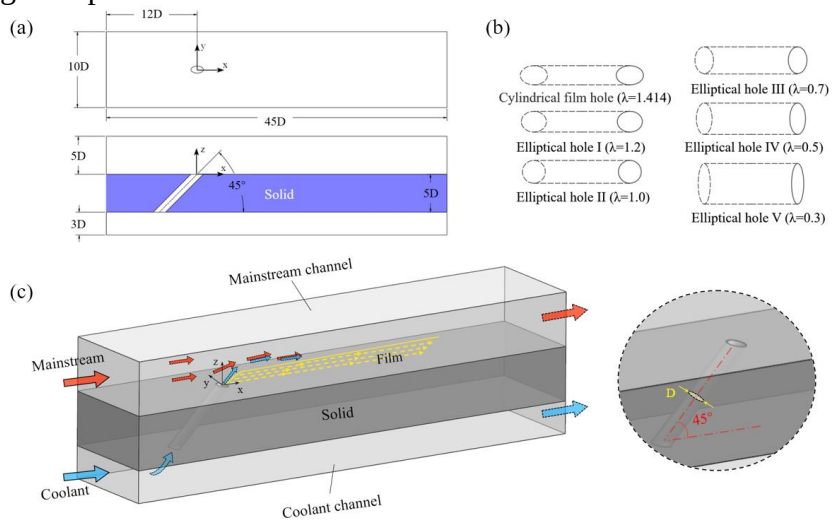

Figure 1: Research Model of Film Cooling: (a) Geometric Model Parameters; (b) Geometric Model of the Film Cooling Hole; (c) Boundary Conditions of the Model.

Fig. 1(a) illustrates the geometric parameters of the analysis model. The coordinate system was centered at the exit of the film cooling hole on the mainstream side, with the positive X-axis aligned along the mainstream flow direction. The geometric description of the orifice of the elliptical hole was based on a cylindrical hole[30]. The cylindrical hole had a diameter D = 0.4 mm, and the flat plate thickness was 5D. Fig. 1(b) shows the six types of elliptical film cooling holes with varying ellipticities studied in this research. The ellipticity λ is defined as the ratio of the major axis a to the minor axis a of the elliptical hole, as given in Equation (1). For the inclined elliptical hole, the ellipticity is 1.414. According to the aforementioned formula, five elliptical hole structures were derived in this study, and their corresponding ellipticities of 0.2, 1.0, 0.7, 0.5, 0.3, respectively.

$$\lambda = \frac{a}{b} \tag{1}$$

The analysis domain model was solved using ANSYS CFX 2021. Following the research by Tu et al. [30], the top and bottom sides of the analysis domain were set as symmetry boundaries. The left and right sides of both the mainstream and coolant regions were defined as periodic walls. The interface between the fluid and solid domains was set in the CHT simulation as a coupled wall. The heat flux and temperature exchange between the fluid and solid at the conjugate coupled wall are defined as follows [31]:

$$T_{m_i} = T_{c_i} \tag{2}$$

$$-k_c \frac{\partial T_{c_i}}{\partial n} = k_m \frac{\partial T_{m_i}}{\partial n} \tag{3}$$

The equations involve fluid temperatures at the mainstream domain T_{m_i} and the cooling domain T_{c_i}, thermal transfer rates of the two domains k_c and k_m, and the normal vector n at the coupled wall. Table 1 lists the boundary settings for the three different air blowing ratios, with the air blowing ratio defined as follows:

$$\mathrm{B}^{\circ} = \frac{\rho_c u_c}{\rho_g u_g} \tag{4}$$

In this equation, the fluid velocities in the main domain and cooling domain are represented by u_g

and u_c, respectively, while the fluid densities in these domains are denoted by ρ_g and ρ_c. The temperatures at the entrances to the primary area (T_m) and cooling domain (T_c) are set to 1600 K and 700 K, respectively. According to previous studies, this temperature ratio accurately reflects the engine's operating temperature[31]. Pressure boundary conditions are applied to both the inlet and outlet boundaries. Here, P_{m1} and P_{c1} represent the total pressures at the inlets of the main domain and cooling domain, respectively, while P_{m2} and P_{c2} denote the static pressures at the outlets. The turbulence intensities of the main and cooling flows are indicated by M_{am} and M_{ac}, respectively.

Table 1: Boundary Conditions of the Flow Domains.

Boundary condition	B = 0.5	B = 1.0	B = 1.5
T_m(K)	1600	1600	1600
P_{m1}(N/m^2)	13.128×10^5	13.128×10^5	13.128×10^5
P_{m2}(N/m^2)	12.1×10^5	12.1×10^5	12.1×10^5
M_{am}(%)	1	1	1
T_c(K)	700	700	700
P_{c1}(N/m^2)	12.45×10^5	12.99×10^5	13.89×10^5
P_{c2}(N/m^2)	12.38×10^5	12.92×10^5	13.82×10^5
M_{ac}(%)	5	5	5

2.2. Verification of the turbulence model and grid independence

The analysis domain model is solved using the shear stress transport (SST) turbulence model combined with the Gamma–Theta transition model. Researchers have confirmed through experiments that the Gamma Theta transition model significantly improves the computational accuracy of the SST turbulence model, making the calculated data more consistent with experimental results[24]. Additionally, the SST turbulence model has been found to perform optimally in solving film cooling models and demonstrates high computational accuracy in heat transfer analysis [20,32].

The analysis domain is meshed with high-quality hexahedral elements using ICEM CFD. The mesh is refined and densified at the entrance and exit of the flow field and near-wall boundary layers. The meshing results are shown in Fig. 2a. The first layer of mesh near the wall satisfies y+ < 1, and the mesh growth rate is kept within 1.1. To guarantee computational precision, the conjugate heat transfer (CHT) simulation uses a conformal mesh with common nodes at the fluid–solid conjugate coupling interface. Based on the comparison of the CHT simulation results for models with different mesh quantities, it can be observed in the mesh independence analysis shown in Fig.2b that the calculated comprehensive cooling efficiency η stabilizes when the number of mesh elements increases to 2.03 million. Therefore, in this study, the number of mesh elements is set to 2.03 million. The comprehensive cooling efficiency η is defined as follows:

$$\eta = \frac{T_g - T}{T_g - T_c} \tag{5}$$

In this equation, T_g is the temperature of the high-temperature gas stream in the main domain, T_c is the temperature of the cooling gas flow in the cooling domain, and T represents the wall temperature of the solid domain. Additionally, in the adiabatic analysis, the adiabatic cooling efficiency η_a is defined as follows:

$$\eta_a = \frac{T_g - T_a}{T_g - T_c} \tag{6}$$

In this context, T_a stands for the temperature at the adiabatic wall, specifically indicating the temperature at the bottom layer of the film cooling.

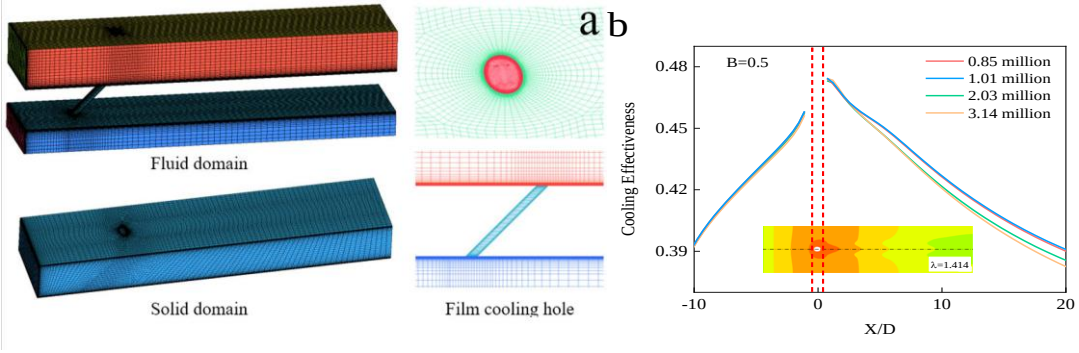

Figure 2: a: Mesh of the Computational Domain; b: Effect of Film Cooling on the Centerline of the Target Wall with a Blowing Ratio (B = 0.5).

3. Results and Discussion

3.1. Analysis of the Cooling Performance of Holes with Different Ellipticities

Fig. 3A displays the distribution of the adiabatic cooling efficiency on the mainstream wall surface for holes of different ellipticities at blowing ratios of 1.5, 1.0, and 0.5. As the blowing ratio increases, the adiabatic cooling effect near the hole outlets of the six hole types decreases to varying degrees. An increased blowing ratio boosts the kinetic energy of the coolant jet, aiding its penetration into the mainstream airflow and the formation of kidney-shaped vortices. These vortices draw in high-temperature flow beneath the film layer, raising the upstream film and diminishing the local cooling effectiveness. Nevertheless, as the hole ellipticity decreases, the impact of this increase in the blowing ratio on the local film cooling effectiveness steadily diminishes. Notably, when maintaining a constant cross-sectional area, the structural geometry of the elliptical hole enables a reduction in the total outflow kinetic energy in the mainstream direction due to its expansion in the transverse direction. Consequently, this mitigates the influence of kidney-shaped vortices on cooling effectiveness.

Fig. 3B also shows the cooling performance of each hole type along the centerline of the mainstream wall surface at three distinct blowing ratios. Fig. 3B (a) indicates that at lower blowing ratios, the variations in the cooling effectiveness in the mainstream direction among the different hole types are minimal, with some differences observed between the X/D ratios of 4 and 15. Due to the low kinetic energy of the coolant jet, the coolant flow maintains good adherence around the hole outlets, resulting in relatively consistent film coverage upstream for each hole type. However, for the same reason, the cooling efficiency of the film rapidly decreases in the central to downstream areas. As the ellipticity of the film cooling hole decreases, the lateral expansion of the geometric shape of the hole jet becomes more dispersed.

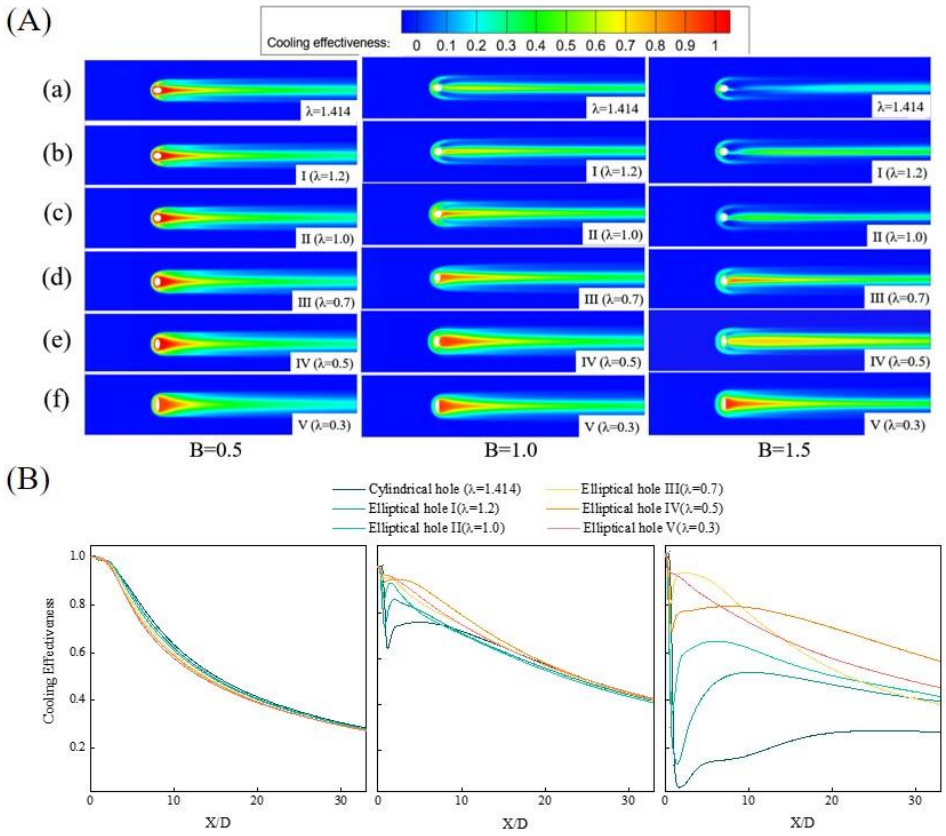

Figure 3: A: The cooling effectiveness of the adiabatic film on the mainstream sidewall surface: (a) λ=1.414; (b) Hole I, λ=1.2; (c) Hole II, λ=1.0; (d) Hole III, λ=0.7; (d) Hole IV, λ=0.5; (d) Hole V, λ=0.3. B: The adiabatic cooling effectiveness varies with the blowing ratio at the centerline of the main sidewall. (a) B = 0.5; (b) B = 1.0; and (c) B = 1.5.

Although this expands the attachment area of the coolant film, it simultaneously reduces the jet's kinetic energy in the streamwise direction. Consequently, Fig. 3B (a) shows that holes with reduced ellipticity disperse more jet kinetic energy in the midstream region, resulting in a more pronounced decrease downstream cooling efficiency. In contrast, Fig. 3B (b) reveals that at moderate blowing ratios, a marked decrease in the cooling effectiveness initially occurs in the upstream portion of the hole outlet. As the ellipticity decreases, the extent of the decrease in cooling efficiency at the aperture exit also decreases. The cooling effectiveness decreases at the hole outlet and then quickly recovers in the upstream region, followed by a further decrease in the midstream region. Consistent with earlier discussions, an increase in the blowing ratio boosts the jet's kinetic energy, causing the uplift of the film at the outlet. However, the lateral expansion of the hole counteracts this effect by dispersing the jet, thus reducing its impact. In Fig. 3B (c), this phenomenon is more evident at high blowing ratios. At high blowing ratios, lateral elliptical holes exhibit a greater overall adiabatic cooling effect than circular and longitudinal elliptical holes. However, in Fig. 3B (c), it is noted that the enhancement of this adiabatic cooling effect does not show a consistent relationship with changes in ellipticity. However, as the ellipticity decreases, the improvement in the adiabatic cooling effectiveness in the mid- to downstream regions is restricted. For example, when λ = 0.3, the cooling effectiveness in the midstream region is considerably greater than that at other ellipticities, but the reduction in cooling effectiveness downstream is much greater. Thus, it is evident that while lateral expansion of the hole geometry significantly disperses the jet, enhancing the film cooling performance upstream, it also intensifies the dissipation of jet kinetic energy, thereby reducing the cooling performance downstream.

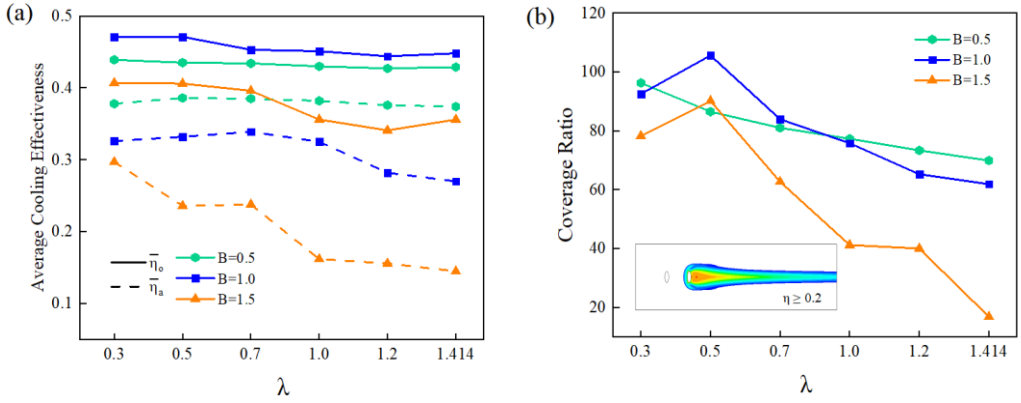

Figure 4: a: The average film cooling effectiveness on the main streamwise wall varies with different elliptical holes. b: Effective film coverage ratio of different elliptical holes.

Fig. 4a displays the mean adiabatic cooling efficiency $\overline{\eta_a}$ and the average comprehensive cooling effectiveness $\overline{\eta_O}$ of the different elliptical holes at the different blowing ratios. As discussed earlier, at low blowing ratios, the cooling effectiveness distributions between elliptical holes are similar, resulting in small differences in the average cooling effectiveness. With an increasing blowing ratio, each hole's average adiabatic cooling effectiveness significantly decreases. Among them, holes with higher ellipticity show a greater reduction in the mean adiabatic cooling efficiency, which is consistent with the influence of aperture geometry changes on the aerodynamic characteristics, as discussed earlier. Moreover, Fig. 4a shows that ellipticity significantly impacts the average comprehensive cooling effectiveness. However, the overall cooling efficiency of film cooling holes results from the cumulative impacts of internal impingement cooling, convective heat transfer around the hole, and external film cooling. Among these, the improvement in cooling effectiveness from internal impingement cooling is notably greater than that from external film cooling. Additionally, the external film detachment caused by high blowing ratios can have adverse effects [20].

Fig. 4a demonstrates a substantial improvement in the adiabatic film cooling efficiency because of internal impingement cooling and convective heat transfer around the hole. Particularly, at high blowing ratios, the relatively intense internal impingement cooling and convective heat transfer around the hole compensate for the external film cooling effectiveness to a greater extent. However, the inadequate cooling effectiveness caused by external film detachment decreases the comprehensive cooling performance at high blowing ratios. Therefore, a moderate blowing ratio (B=1.0) actually results in the best comprehensive cooling performance when combined with effective external cooling and strong internal impingement cooling with convective heat transfer around the hole. Additionally, changes in the hole geometry significantly influence the convective heat transfer around the hole, with the comprehensive cooling effectiveness gradually decreasing as the ellipticity increases. Specifically, compared to an ellipticity of 0.3, an ellipticity of 0.5 contributes more significantly to the comprehensive cooling effectiveness through internal impingement cooling and convective heat dissipation around the hole.

The film coverage on the wall surface is also a crucial metric for assessing the efficacy of cooling film cooling holes. The ability to prevent thermal corrosion requires the film to have good coverage. To accurately study the film coverage effect of elliptical holes, this paper defines the effective film attachment region as the area where the adiabatic cooling effectiveness η is greater than or equal to 0.2. The effective film coverage ratio is defined as follows:

$$A_f = \frac{a_f}{a_h} \tag{7}$$

In this equation, a_f represents the total area of the effective film attachment region, and a_h denotes the cross-sectional area of the film cooling hole. At a low blowing ratio (B=0.5), elliptical hole V (with λ=0.3) has the largest A_f, indicating good film attachment. As the ellipticity of the hole increases, the effective film coverage ratio on the wall surface significantly decreases. At a low blowing ratio (B=0.5), the lateral expansion of the hole shape enhances the film coverage effectiveness. At moderate to high blowing ratios (B=1.0, B=1.5), elliptical hole IV (λ =0.5) exhibited the best film coverage effectiveness. As the ellipticity increases or decreases, the A_f of the other hole shapes significantly decreases. Clearly, once the lateral expansion of the elliptical hole reaches a certain extent, the attachment of the film on the wall surface is inhibited. Additionally, at high blowing ratios, the A_f values of all six hole shapes significantly decrease. The effective coverage ratio of elliptical hole V (λ =0.3) is second only to that of elliptical hole IV (λ =0.5). The difference between the two is that the optimal film coverage area for elliptical hole V is concentrated around the hole exit and upstream regions. In contrast, its downstream film coverage effectiveness is poorer (as shown in Fig. 4a). This is because further lateral expansion of the elliptical hole reduces the loss of jet kinetic energy, leading to more pronounced jet lift-off and faster energy dissipation of the lateral jet, which weakens the coverage efficiency downstream of the film.

In summary, elliptical holes demonstrate an optimal cooling efficiency on the wall surface under moderate blowing ratios. Among the six types of elliptical holes examined, the elliptical hole with an ellipticity of λ=0.5 shows the best mix of effective film coverage and overall cooling effectiveness, proving to be the most effective type for cooling purposes.

3.2. Analysis of the flow field characteristics of holes with different ellipticities

The previous section provided a preliminary analysis of how ellipticity influences the aerodynamics and heat transfer properties of film cooling, discussing the impacts on cooling performance. The ellipticity significantly affects the cooling effectiveness of the holes under moderate to high blowing ratios. To delve deeper into the underlying mechanisms, this section comprehensively analyzes the flow field characteristics of holes with varying ellipticities. Based on Fig. 3B, holes with distinct characteristics are selected for discussion, including circular holes (λ=1.414), elliptical hole II (λ=1.0), elliptical hole IV (λ=0.5), and elliptical hole V (λ=0.3).

Fig. 5A depicts the velocity distribution on the central plane (Y/D = 0) under moderate to high blowing ratios, the three-dimensional streamlines in the upstream flow field, and the adiabatic cooling effectiveness at the critical section (X/D = 3) and on the wall. Fig. 5A(a) shows the flow field characteristics of the circular hole when B=1.0. The cooling stream interacts with the mainstream upon ejection from the hole, creating shear vortices on either side of the hole opening, which are aligned with the mainstream flow direction (as highlighted in the annotated area of the figure). As the flow progresses downstream, substantial mixing of the high-temperature mainstream with the jet disperses these shear vortices. Above the wall, kidney-shaped vortices form (as depicted at X/D = 3). The small vortices on both sides of the hole result primarily from the horseshoe vortices formed by mixing a small amount of jet flow at the forward edge of the hole with the mainstream flow, which is diverted sideways due to jet stripping. By examining the changes in flow structure at the hole opening and correlating them with the distribution of cooling effectiveness, it is observed that the cooling effectiveness in the hole opening region and downstream wall area is closely tied to the behavior of the shear vortices and kidney-shaped vortices above. The shear vortices generated at the circular hole opening demonstrate relatively low intensity and are carried away from the hole opening by the mainstream flow, leading to reduced cooling effectiveness at the hole opening. This phenomenon gives rise to kidney-shaped vortices farther from the wall at the section, thereby decreasing the downstream cooling effectiveness.

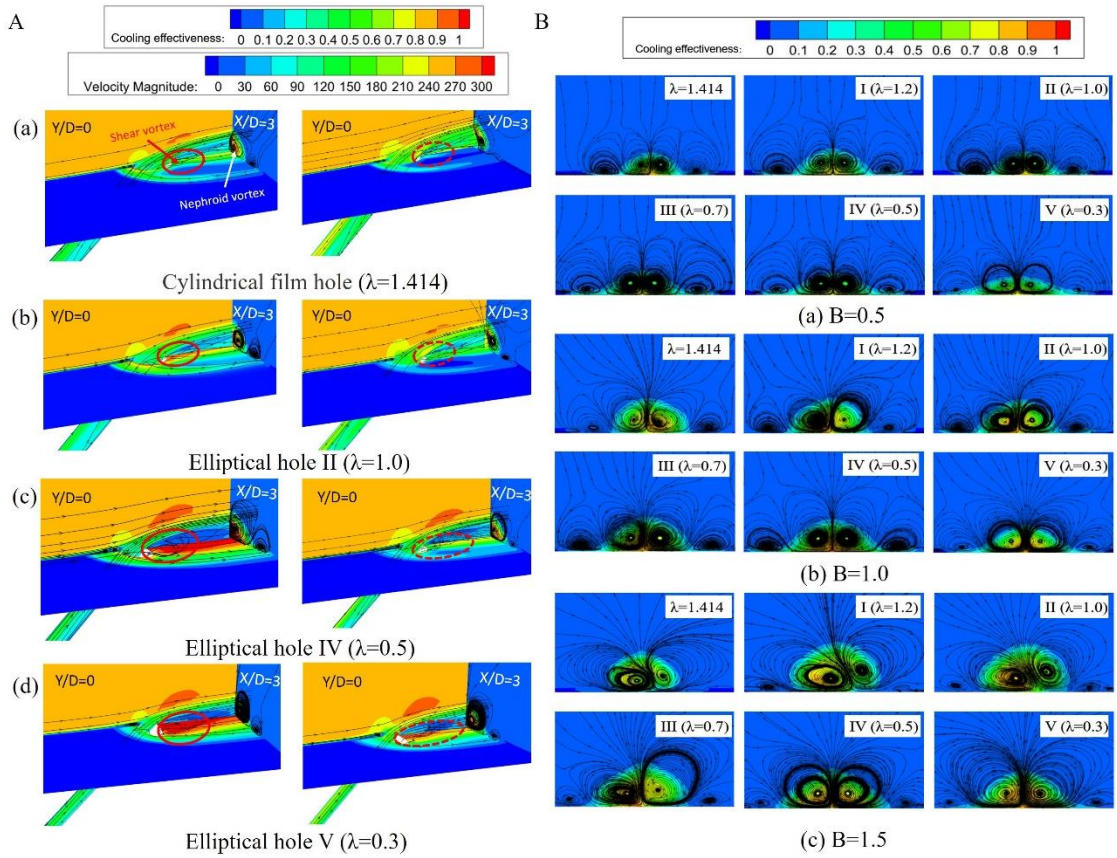

Figure 5: A: The velocity distribution on the center plane (Y/D = 0) and the dispersion of the adiabatic cooling efficiency on the wall and at the critical section (X/D = 3): (a) λ= 1.414; (b) λ= 1.0; (c) λ= 0.5; and (d) λ= 0.3. B: Cooling effectiveness and streamline distribution on the X/D = 5 section.

Compared to the streamline of the circular hole jet in Fig. 5A(a), in Fig. 5A(b-d), with decreasing ellipticity, the curvature of the exit jet becomes more pronounced, and the streamlines are closer to the wall, reducing the kinetic energy of the jet and facilitating its attachment to the wall. However, in Figs. 5A(c, d), the shear vortices on both sides of the smaller elliptical hole openings are more pronounced, leading to an increase in kidney-shaped vortices in the X/D = 3 section. In Fig. 5A(d), the curvature of the jet at the opening of elliptical hole V is the most pronounced, causing the shear vortices on both sides of the hole to form in a narrower space. This results in fewer vortices forming at X/D = 3 compared to elliptical hole IV, significantly enhancing the film cooling capability at the hole entrance. This also explains why in Figs. 5A(b, c), the cooling effectiveness at the outlet of elliptical hole V is noticeably greater than that at the outlet of elliptical hole IV, particularly at high blowing ratios.

When B = 1.5, the jet's kinetic energy upon exit increases, resulting in quicker injection into the mainstream. This results in varying degrees of uplift of the vortices above the wall for all four types of elliptical holes displayed in the figure. Notably, the circular hole and elliptical hole II show kidney-shaped vortices at the X/D = 3 section that completely detach from the wall, resulting in reduced cooling effectiveness in the upstream region of the film. At high blowing ratios, the size and intensity of the shear vortices around elliptical hole IV decrease markedly, diminishing the cooling effectiveness in the hole opening region. This is also evident in Fig. 5A(b) and Fig. 5A(c), where the cooling effectiveness in the hole opening region is lower at high blowing ratios than at moderate

blowing ratios. Conversely, elliptical hole V exhibits the least sensitivity to changes in the blowing ratio among the hole types studied. Shear vortices remain attached to the hole opening region, and the increase in the size of the kidney-shaped vortices at the section under high blowing ratios is relatively minor and remains closer to the wall, enhancing the film's coverage effectiveness.

The changes in the flow field structure on the wall were analyzed to investigate the cooling characteristics downstream along the flow direction. With the dispersion and recombination of shear vortices, kidney-shaped vortices form above the wall. Fig. 5B illustrates the cooling effectiveness and streamline distribution in the X/D = 5 section under varying blowing ratios. The cooling airflow mixes with the mainstream gas, forming a pair of counterrotating vortices above the wall. Based on the distribution of cooling effectiveness in this section, it is evident that central kidney-shaped vortices primarily achieve wall cooling.

When B = 0.5, there is no noteworthy variation in the cooling effectiveness among the six hole types in the X/D = 5 section. However, the kidney-shaped vortices formed by elliptical hole V (λ=0.3) are relatively larger and less intense. Larger vortices tend to draw in more hot gas from above the wall, reducing the film's cooling effectiveness. This is corroborated by the cooling effectiveness curve in Fig. 5B(a), where the film cooling effectiveness of elliptical hole V is consistently lower than that of the other hole types when B = 0.5.

When B = 1.0 and B = 1.5, with increasing blowing ratios, the size of the kidney-formed vortices on the wall notably increases, showing a tendency to lift off. The sizes of the kidney-formed vortices formed by the circular hole and elliptical holes I, II, and III vary. However, in areas with higher cooling effectiveness on the section, which are mainly located on the side with smaller vortices, the larger-sized vortices entrain a significant amount of hot gas and show slight uplift. Consequently, the mixed cooling gas has a reduced impact on the wall (as illustrated in Fig. 5B(b) and Fig. 5B(c)). This phenomenon leads to a continuous uplift of the vortices, with subsequent cooling mainly supported by one side of the vortices, greatly reducing the effectiveness of the film on the wall. Moreover, at moderate to high blowing ratios, elliptical holes IV and V continue to generate a pair of smaller kidney-shaped vortices above the wall. This configuration sustains the adhesion of the film to the wall while reducing the interference of high-temperature gas with film cooling, thereby maintaining effective cooling. Among these, the kidney-shaped vortices formed by elliptical hole V are slightly larger, and the intensity of the vortex core is relatively weaker, resulting in lower cooling effectiveness than that of elliptical hole IV. Hence, in the cooling effectiveness distribution shown in Fig. 5B(b) and Fig.5B(c), the cooling efficiency of elliptical aperture V in the midstream to downstream regions is lower than that of elliptical hole IV.

4. Conclusions

This study explored the adiabatic and overall cooling characteristics of elliptical film cooling holes with varying ellipticities. The cooling effectiveness of six elliptical hole configurations was compared and analyzed through numerical simulations at low, medium, and high blowing ratios. This study also integrated the streamline distribution and flow characteristics within the flow field to elucidate the cooling mechanisms of elliptical holes and the differences in flow field structures among various hole types. The principal conclusions drawn are as follows:

- At medium blowing ratios, elliptical holes significantly impact the film cooling performance. As the ellipticity decreases, the lateral expansion of the holes increases, which reduces the dissipation of the jet kinetic energy at the hole outlet. This leads to enhanced adhesion and coverage of the film, significantly improving the overall cooling performance. Among these, elliptical holes with an ellipticity of λ=0.5 demonstrate the highest film effectiveness and overall cooling performance, making them the optimal hole type for these conditions.

• At a medium blowing ratio, the hole structure changes due to the reduction in the ellipticity, altering the flow structure within the hole. This leads to the contraction of the low-speed region at the center of the hole and the generation of a pair of reverse vortices by the high-velocity airflow surrounding the hole. When $\lambda = 0.3$, only two pairs of smaller reverse vortices are formed. As the vortex strength decreases on both sides, the jet's kinetic energy exiting the hole increases significantly, resulting in a bending coil at the exit. This hampers the formation of subsequent shear and kidney-shaped vortices, thereby enhancing the coverage and cooling performance of the air film. Moreover, when the transverse expansion scale of the elliptical holes exceeds a certain range, i.e., when the ellipticity is ≤ 0.3, the cooling efficiency of the elliptical holes is suppressed.

Acknowledgements

This work was supported by National Natural Science Foundation of China [No. 52375153], the Natural Science Basic Research Program of Shaanxi [2023-JC-YB-068], the Youth Innovation Team of Shaanxi Universities (2024).

References

[1] Z.Y. Liu, W. Zhu, L. Yang, Y.C. Zhou, Numerical prediction of thermal insulation performance and stress distribution of thermal barrier coatings coated on a turbine vane, Int. J. Thermal Sci. 158 (2020) 106552. https://doi.org/10.1016/j.ijthermalsci.2020.106552

[2] L. Liu, S. Fu, Z. Hu, J. Wu, J. Chen, X. Jin, X. Fan, Thermo-mechanical analysis of TBC-film cooling system under high blowing ratio considering the effects of curvature, Surf. Coat. Technol. 470 (2023) 129826. https://doi.org/10.1016/j.surfcoat.2023.129826

[3] M. Zhao, Y. Bian, J. Xu, T. Ye, Large eddy simulation of film cooling with different upstream obstacles, Int. J. Thermal Sci. 161 (2021) 106722. https://doi.org/10.1016/j.ijthermalsci.2020.106722

[4] X. Huang, J. Pu, T. Zhang, J.-H. Wang, W.-L. Wu, X.-Y. Wu, Effect of length-to-diameter ratio on film cooling and heat transfer performances of simple and compound cylindrical-holes in transverse trenches with various depths, Int. J. Heat Mass Transfer 185 (2022) 122328. https://doi.org/10.1016/j.ijheatmasstransfer.2021.122328

[5] P. Chen, L. Wang, X. Li, J. Ren, H. Jiang, T. Simon, Enhancement of film cooling effectiveness using dean vortices, J. Turbomach. 142 (2020) 011005. https://doi.org/10.1115/1.4045336

[6] D.W. MacPhee, A. Beyene, Impact of air quality and site selection on gas turbine engine performance, J. Energy Resour. Technol. 140 (2018) 020903. https://doi.org/10.1115/1.4038118

[7] J. Pu, W. Wang, J.-h. Wang, W.-l. Wu, M. Wang, Experimental study of free-stream turbulence intensity effect on overall cooling performances and solid thermal deformations of vane laminated end-walls with various internal pin–fin configurations, Appl. Thermal Eng. 173 (2020) 115232. https://doi.org/10.1016/j.applthermaleng.2020.115232

[8] H. Du, Z. Mei, J. Zou, W. Jiang, D. Xie, Conjugate heat transfer investigation on swirl-film cooling at the leading edge of a gas turbine vane, Entropy 21 (2019) 1007. https://doi.org/10.3390/e21101007

[9] G. Zhang, G. Xie, B.A. Sunden, Comparative analysis on the film cooling mechanisms of elliptical and cylindrical holes with 90° compound angle, Int. J. Numeric. Meth. Heat Fluid Flow 31 (2021) 192-215. https://doi.org/10.1108/HFF-10-2019-0764

[10] C. Zhang, W. Wang, Z. Wang, Z. Tong, Conjugate heat transfer simulation of overall cooling performance for cratered film cooling holes, Machines 10 (2022) 395. https://doi.org/10.3390/machines10050395

[11] M. Zhang, Determination of film cooling effectiveness and heat transfer coefficient simultaneously on a flat plate, Energies 15 (2022) 4144. https://doi.org/10.3390/en15114144

[12] J.Y. Jeong, Y.R. Jo, M.S. Kang, Y.J. Kang, J.S. Kwak, Film cooling effectiveness and flow structures of butterfly-shaped film cooling hole configuration, J. Thermal Sci. Eng. Appl. 16 (2024) 031009. https://doi.org/10.1115/1.4064430

[13] J.H. Liu, Y.B. Liu, L. Liu, Film cooling modeling of a turbine vane with multiple configurations of holes, Case Stud. Thermal Eng. 11 (2018) 71-80. https://doi.org/10.1016/j.csite.2018.01.001

[14] F. Gao, X. Duan, L. Zhang, J. Chang, Influence of groove structure on film cooling, Energy Rep. 8 (2022) 136-151. https://doi.org/10.1016/j.egyr.2022.09.129.

[15] J. Fu, Y. Cao, C. Zhang, J. Zhu, Investigation of the conjugate heat transfer and flow field for a flat plate with combined film and impingement cooling, J. Thermal Sci. 29 (2020) 955-971. https://doi.org/10.1007/s11630-020-1233-2

[16] G. Chen, Y. Liu, Y. Rao, J. He, Y. Qu, Numerical investigation on conjugate heat transfer of impingement/effusion double-wall cooling with different crossflow schemes, Appl. Thermal Eng. 155 (2019) 515-524.

https://doi.org/10.1016/j.applthermaleng.2019.04.019
[17] Y.S. Kim, J.Y. Jeong, J.S. Kwak, H. Chung, The effects of hole arrangement and density ratio on the heat transfer coefficient augmentation of fan-shaped film cooling holes, Energies 14 (2021) 186. https://doi.org/10.3390/en14010186
[18] K. Kusterer, N. Tekin, T. Wüllner, D. Bohn, T. Sugimoto, R. Tanaka, M. Kazari, Nekomimi film cooling holes configuration under conjugate heat transfer conditions, in: ASME Turbo Expo 2014: Turbine Technical Conference and Exposition, Düsseldorf, Germany, American Society of Mechanical Engineers, 2014, p. V05BT13A028. https://doi.org/10.1115/GT2014-25845.
[19] J. Wang, W. Wang, G.-c. Li, D. Luo, J. Wu, Numerical study of the cooling performance of rupert-shaped film cooling holes, Int. J. Thermal Sci. 198 (2024) 108859. https://doi.org/10.1016/j.ijthermalsci.2023.108859
[20] W. Zhou, Q. Deng, W. He, J. He, Z. Feng, Conjugate heat transfer analysis for composite cooling structure using a decoupled method, Int. J. Heat Mass Transfer 149 (2020) 119200. https://doi.org/ 10.1016/j.ijheatmasstransfer.2019.119200
[21] Y. Liu, Y. Rao, L. Yang, Y. Xu, A. Terzis, Flow and heat transfer characteristics of double-wall cooling with multi-row short film cooling hole arrangements, Int. J. Thermal Sci. 165 (2021) 106878. https://doi.org/ 10.1016/j.ijthermalsci.2021.106878
[22] Z. Wang, D. Wang, Z. Wang, Z. Feng, Heat transfer analyses of film-cooled HP turbine vane considering effects of swirl and hot streak, Appl. Thermal Eng. 142 (2018) 815-829. https://doi.org/10.1016/j.applthermaleng.2018.07.044
[23] M. Wang, H. Zhu, C. Liu, T. Guo, L. Zhang, N. Li, Numerical analysis and design optimization on full coverage film-cooling for turbine guided vane, Eng. Appl. Comput. Fluid Mech. 16 (2022) 904-936. https://doi.org/ 10.1080/19942060.2021.2019127
[24] M. Wang, H. Zhu, C. Liu, T. Guo, Z. Wu, N. Li, Structure improvement on turbine guided vane cooling system based on conjugate heat transfer, Int. J. Thermal Sci. 172 (2022) 107332. https://doi.org/10.1016/j.ijthermalsci.2021.107332
[25] C. Liu, G. Xie, R. Wang, L. Ye, Study on analogy principle of overall cooling effectiveness for composite cooling structures with impingement and effusion, Int. J. Heat Mass Transfer 127 (2018) 639-650. https://doi.org/ 10.1016/j.ijheatmasstransfer.2018.07.085
[26] M. Silieti, A.J. Kassab, E. Divo, Film cooling effectiveness: Comparison of adiabatic and conjugate heat transfer CFD models, Int. J. Thermal Sci. 48 (2009) 2237-2248. https://doi.org/10.1016/j.ijthermalsci.2009.04.007
[27] J. Zhou, X. Wang, J. Li, Influences of effusion hole diameter on impingement/effusion cooling performance at turbine blade leading edge, Int. J. Heat Mass Transfer 134 (2019) 1101-1118. https://doi.org/ 10.1016/j. ijheatmasstransfer.2019.02.054
[28] G. Xie, C.-l. Liu, L. Ye, R. Wang, J. Niu, Y. Zhai, Effects of impingement gap and hole arrangement on overall cooling effectiveness for impingement/effusion cooling, Int. J. Heat Mass Transfer 152 (2020) 119449. https://doi.org/ 10.1016/j.ijheatmasstransfer.2020.119449
[29] S.K. Hong, D.H. Lee, H.H. Cho, Heat/mass transfer in rotating impingement/effusion cooling with rib turbulators, Int. J. Heat Mass Transfer 52 (2009) 3109-3117. https://doi.org/10.1016/j.ijheatmasstransfer.2009.01.031
[30] Z. Tu, J. Mao, X. Han, Numerical study of film cooling over a flat plate with anisotropic thermal conductivity, Appl. Thermal Eng. 111 (2017) 968-980. https://doi.org/10.1016/j.applthermaleng.2016.09.170
[31] J. Jiang, L. Jiang, Z. Cai, W. Wang, X. Zhao, Y. Liu, Z. Cao, Numerical stress analysis of the TBC-film cooling system under operating conditions considering the effects of thermal gradient and TGO growth, Surf. Coat. Technol. 357 (2019) 433-444. https://doi.org/10.1016/j.surfcoat.2018.10.020
[32] Z. Liu, L. Ye, C. Wang, Z. Feng, Numerical simulation on impingement and film composite cooling of blade leading edge model for gas turbine, Appl. Thermal Eng. 73 (2014) 1432-1443. https://doi.org/10.1016/j. applthermaleng.2014.05.060